Modeling, Detection, and Disambiguation of Sensor Faults for Aerospace Applications

Edward Balaban, *Member, IEEE*, Abhinav Saxena, *Member, IEEE*, Prasun Bansal, Kai F. Goebel, *Member, IEEE*, and Simon Curran

***Abstract*—Sensor faults continue to be a major hurdle for systems health management to reach its full potential. At the same time, few recorded instances of sensor faults exist. It is equally difficult to seed particular sensor faults. Therefore, research is underway to better understand the different fault modes seen in sensors and to model the faults. The fault models can then be used in simulated sensor fault scenarios to ensure that algorithms can distinguish between sensor faults and system faults. The paper illustrates the work with data collected from an electromechanical actuator in an aerospace setting, equipped with temperature, vibration, current, and position sensors. The most common sensor faults, such as bias, drift, scaling, and dropout were simulated and injected into the experimental data, with the goal of making these simulations as realistic as feasible. A neural network-based classifier was then created and tested on both experimental data and the more challenging randomized data sequences. Additional studies were also conducted to determine sensitivity of detection and disambiguation efficacy with respect to severity of fault conditions.**

***Index Terms*—Fault diagnosis, modeling, transducers.**

I. Introduction

SENSORS play a central role in realizing the full benefits of cost and performance in modern aerospace systems. The degree of autonomy of these systems is highly correlated with the number of sensors used in them. Features like guaranteed uptime also mandate continuous state analysis with a respective increase in use of sensors.

However, as such systems have become more reliable as a whole, sensors have attained the reputation as being the "weak link." Indeed, sensor failures have been responsible for highly publicized system breakdowns such as aborted takeoffs of the space shuttle. For that reason, particularly for those systems that require very high overall reliability combined with the need to keep weight low, there is a reluctance to add more sensors. Where sensors are used, they are configured with up to quadruple redundancy in order to be able to deal with sensor failure—which, as in the cited case, may not prevent operational disruption (depending also on the fault handling logic). This, in contrast to the general trend of increasing system sophistication, has hamstrung the proliferation of health management systems and, consequently, their potential technical advances.

In addition to increased weight, redundant sensors are not always feasible due to considerations of cost, space constraints, electrical/power constraints, and increased complexity. Any new sensor has to "work its way on-board".

It is, therefore, critical to have an understanding of how sensors fail in order to mitigate the effects of their off-nominal behavior. While sensor fault detection and diagnosis are well addressed in the literature, there is no consensus on classification and nomenclature for sensor faults. Equally sparse are research efforts on characterization of the various classes of sensor faults and efforts to develop realistic fault models. Such models would allow simulation of sensor fault effects and their impact on the systems they are used in. They would also allow the study of sensor suit development; testing of fault detection, isolation, and recovery algorithms; and assessment of prognostic algorithm performance.

This paper starts with classifying and summarizing fault modes for the most common sensor types used in the aerospace industry. A brief overview of state-of-the-art diagnostic techniques for sensor faults is then provided. The discussion then shifts to describing experiments conducted by the team in simulating and diagnosing sensor faults. Finally, results of the study are discussed and plans for future work outlined.

II. Sensor Fault Modes

Success of any health monitoring system depends heavily on reliability of employed sensors. In abstraction, a sensor fault may be defined as an unexpected deviation in the observed signal output in the absence of any anomalous condition in the system under test. Sensor faults occur due to various reasons, such as manufacturing inefficiencies, wear and tear with long-term usage, incorrect calibration, or mishandling. That often results in some physical deviation from design specifications within the sensor body, which in turn leads to unexpected outputs. From a fault-tolerant control systems point of view, it is usually sufficient to identify the erroneous behavior of a sensor such that no unintended feedback is sent to the controller. System health monitoring is more concerned with the type of deviation observed from the normal expected output, irrespective of the actual physical damage that causes it. However, given the central role that sensor faults play in advancing system health management, it is imperative to have

Manuscript received October 01, 2008; revised May 13, 2009; accepted June 17, 2009. Current version published October 28, 2009. This work was supported in part by the NASA Aerospace Technology (AST) Integrated Vehicle Health Management (IVHM) Program. The associate editor coordinating the review of this paper and approving it for publication was Prof. Jakoby Bernhard.

E. Balaban and K. F. Goebel are with NASA Ames Research Center, Moffett Field, CA 94035 USA (e-mail: edward.balaban@nasa.gov; kai.goebel@nasa.gov).

A. Saxena is with the Research Institute for Advanced Computer Science, NASA Ames Research Center, Moffett Field, CA 94035 USA (e-mail: abhinav.saxena@nasa.gov).

P. Bansal is with Mission Critical Technologies, Inc, NASA Ames Research Center, Moffett Field, CA 94035 USA (e-mail: pbansal@mail.arc.nasa.gov).

S. Curran is with Moog Inc., East Aurora, NY 14052 USA (e-mail: scurran@moog.com).

Digital Object Identifier 10.1109/JSEN.2009.2030284

a good understanding of the various failure mechanisms within the sensors. Mapping failure mechanisms to resulting behaviors is critical to properly model sensor faults.

One can establish five basic behavioral categories for sensor faults.

Bias: A constant offset from the nominal sensor signal statistics. Another way to describe bias is as the sensor output at zero input. Bias can occur due to incorrect calibration or physical changes in the sensor system. The governing equation is $Y_f = X + \beta + \text{noise}$, where β is the constant offset value. A time variant β results in drift failures.

Drift: A time-varying offset from the nominal statistics of the sensor signal. Generally, only linear drifts have been modeled in the literature. However, a nonlinear drift may be possible. Drift failures may be represented as $Y_f = X + \delta(t) + \text{noise}$, where $\delta(t)$ is the time-varying offset factor.

Scaling (or Gain Failure): Magnitudes are scaled by a factor $\alpha(t)$, where the form of the waveform itself does not change [1]. Scaling can be represented by $Y_f = \alpha(t) * X + \text{noise}$, where $0 < \alpha(t) < \infty$ is a scaling constant that may be time-varying.

Noise: A random time series is observed. For analytical simplicity, it is usually assumed that the noise is zero-mean unless some information is available otherwise. It may be represented as $Y_f = \text{noise}$.

Hard Fault: The sensor output is stuck at a particular level expressed by $Y_f = C + \text{noise}$, where C is a constant. In general there are two subcategories for hard failures.

1) Loss of Signal: represents the complete loss of sensor data where the output from the sensor is zero $(C = 0)$ [1].
2) Stuck Sensor: represents the situation where sensor output is stuck at a constant value.

Intermittents: Deviations from normal readings appear and disappear several times from the sensor signal. The frequency of such signatures is generally random. Intermittents can appear in any of the failure modes described above. Due to their random nature, they are the most difficult to track, identify, and account for in diagnostics algorithms.

Other categorizations exist—for example, one that rates the quality of the sensor faults [2]. In particular, tame faults, are fault signals that are both close to nominal signal range and somehow correlated to it [1]. Faults such as bias and drift may fall into this category. Additive faults (like bias and drift) have been also classified into deterministic (constant offset) or semi-deterministic (offsets jump at random intervals and with random amplitudes) [3].

III. Sensed Phenomena

To be able to better model sensor faults, it is important to have an insight into the basic operating principles of the common sensors and the most common fault mechanisms. The phenomena discussed here include only those of most interest to aerospace systems, i.e., the ones encountered in temperature, acceleration, pressure, strain, force, load, current, and position measurements. Several other types of sensors commonly used in aerospace applications, such as attitude, direction, radiation, flow, and others, are left for future studies.

Measurements done by a sensor rely on a particular physical property or behavior of materials. With a suitable infrastructure, these properties can be used to sense/measure several distinct phenomena. For instance, a resistance strain gage can be used to measure strain, stress, loads, or pressure, depending on the application. The mechanism of a particular type of fault and its frequency depends, of course, on the physical design of the sensor. The sensor mechanisms covered and their corresponding uses (in italics) are as follows.

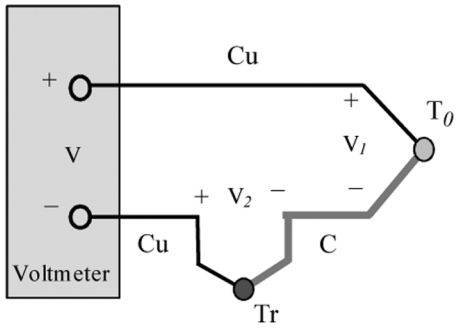

Fig. 1. Thermocouple with external reference junction [6].

1) Thermocouples: *temperature*.
2) Resistance temperature detectors (RTDs): *temperature*
3) Piezoelectric: *acceleration, vibrations, pressure, strain, force*
4) Piezoresistive: *strain, force, pressure, acceleration*
5) Resistive strain: *strain, force, pressure*
6) Hall effect: *current, linear displacement*
7) Magnetostrictive effects: *linear displacement*
8) LVDT: *linear displacement, acceleration*

This list is certainly not complete, but is representative of the more commonly used sensors. Finally, it needs to be mentioned that while the root causes of a sensor fault can be either a failure of the sensing mechanism itself or of the electrical system interpreting the data, only the former cases are discussed in this paper.

A. Thermocouples

Thermoelectric electromagnetic force (EMF) is created in the presence of a temperature difference between two different metals or semiconductors. Thermocouples use this phenomenon, called the Seebeck effect [4], to detect the temperature difference between two sources. A thermocouple circuit consists of two metals, e.g. copper and constantan, with two junctions at temperature $\mathrm{T_o}$ (test junction) and $\mathrm{T_r}$ as reference temperature (Fig. 1). Thermocouples have the widest temperature range of all sensor technologies, -200 to over 2000 °C, and can be used in a wide variety of environments [5].

Faults in Thermocouples:

1) Degradation, corrosion or breakage of junction leading to bias, scaling, intermittent and/or complete failure [6].
2) Inhomogeneous changes in composition of the material taking place due to long exposures to high temperatures, resulting in thermoelectric drift [7], [8].
3) When a thermocouple is bonded to a test surface, degradation of this bond may lead to the junction being at a lower temperature than the body, thus causing a bias.
4) A short (or degradation) in the lead wires can lead to complete failure, bias, or drift [4].

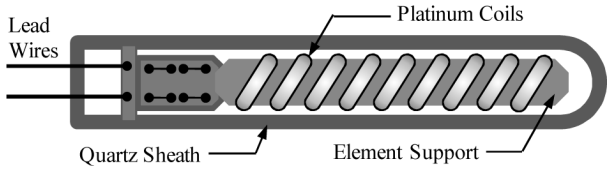

Fig. 2. A standard platinum resistance thermometer [5].

5) Change in the reference temperature leading to bias [6].
6) Change in the thickness of the conducting leads causing a change in resistance, leading to a scaling error.

B. Resistance Temperature Detectors (RTDs)

In an RTD, resistance increases with rise in temperature [4] due to the positive temperature coefficient of electrical resistance of metals. Precision RTDs consist of a thin insulated platinum wire encapsulated in a ceramic or metallic casing (Fig. 2). These casings are then immersed into the fluid or bonded to the surface for temperature measurement. Their normal operation range is roughly -180 °C to 650 °C. In this range they are both more accurate and have more linear characteristics than thermocouples [4]. No reference temperature is needed for the RTDs, but they have to be calibrated carefully at a particular temperature.

Faults in RTDs:

1) Overtime exposure to high temperatures can cause a drift in the values of the RTD to several degrees per year [4].
2) A current passing through the RTD causes self heating of the element that can lead to a bias in the readings [4], [9].
3) Thin-film RTDs experience change in resistance due to surface stresses, which can lead to a bias in the readings.
4) Shock and vibration put strain on resistive wire and change its characteristics, leading to drift [4].
5) Degradation of insulation can cause a short between the coils and result in a lower resistance reading, leading to bias [4].

C. Piezoelectric Sensors

Piezoelectricity is the ability of some materials (certain crystals and ceramics) to generate an electric potential in response to applied mechanical stress. A typical piezoelectric sensor consists of a piezoelectric crystal which is bonded to the surface of interest. Electrodes are connected to the either end of the crystal to sense the electric potential (charge), which can then be related to the stress experienced by the crystal—using piezoelectric and stress coupled equations (Fig. 3). They have a wide frequency range, from 0.01 Hz to 1 MHz [5], and temperature range from -270 °C to $+650$ °C.

Depending on the type of stress applied, a piezoelectric crystal can be used for sensing the following properties [4].

1) Accelerations, from the stress induced in the piezoelectric crystal by a seismic mass (compression, flexure, or shear modes).
2) Vibrations, when mounted directly onto a surface.
3) Strain, when a thin piezoelectric crystal is bonded to a surface.

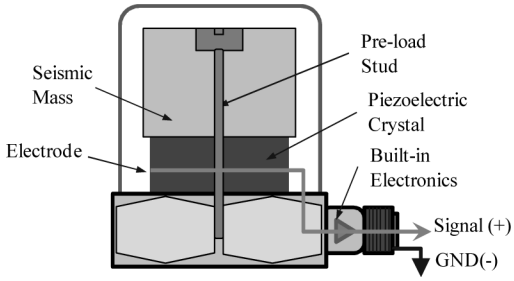

Fig. 3. Piezoelectric accelerometer in compression mode [5].

4) Pressure, either sensed directly by a piezoelectric disk (for high pressure applications) or via strains induced in a diaphragm.
5) Forces, by transmitting them directly through the crystal.

Faults in Piezoelectric Sensors:

1) Debonding due to degradation of the interface between the piezoelectric crystal and the substrate (or the seismic mass) over time can lead to either lower stresses being transferred between them resulting in a scaling error (scale factor < 1) or a change in the frequency response of the crystal, which may, in turn, affect high-frequency behavior of the sensor [10].
2) Cracking of the crystal due to fatigue or shock causes scaling of the outputs from the sensor or a frequency shift of the sensor [11].
3) Depolarization of the crystal takes place if the crystal is subjected to temperatures above the operating range, even for a small time, that can result in a partial or complete loss of sensing capabilities [12].
4) Electric or mechanical fatigue of the crystal over time causes loss of polarization of the crystal, leading to scaling errors in the sensor [12].
5) Loss of contact between the crystal and the lead wires over time due to fatigue or shock can lead to intermittent or complete failure.
6) Temperature variations can lead to a change in the electromechanical properties of the crystals, resulting in bias or drift.

D. Piezoresistive Sensors

The piezoresistive effect is the change in electrical resistance of a material due to applied mechanical stress (which is different from the change in resistance due to dimensional changes, as in a strain gage). Ceramics (or semiconductors) are typically used as the sensing materials as they have high gage factors (Fig. 4). Piezoresistive sensors can be used in static applications and moderately high frequencies up to 2500 Hz [4] and in thermal environments as high as 540 °C [5]. Their operating range is up to 25 G and they can withstand shocks of up to 2000 G [9]. The principles of operation of piezoresistive sensors are the same as that of piezoelectric sensors, with the difference in the frequency range and shock characteristics. Piezoresistive sensors can be configured in the same ways as piezoelectric ones—to sense accelerations, forces, strains, pressures, and low-frequency vibrations.

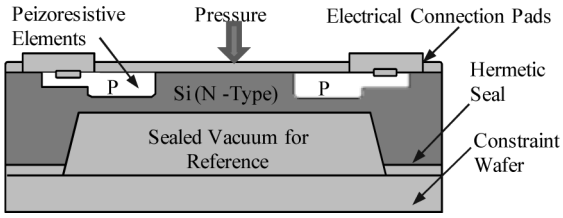

Fig. 4. An absolute pressure sensor with a hermetically sealed vacuum reference chamber on one side of the sensing element [5].

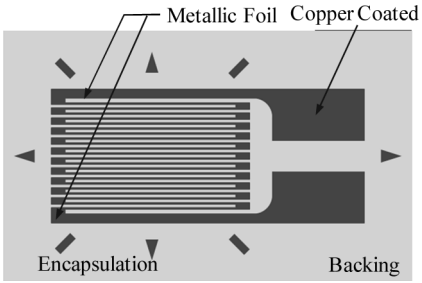

Fig. 5. A typical foil strain gage [13].

Faults in Piezoresistive Sensors:

1) Debonding of the interface between the piezoresistive element and the substrate can lead to a lower degree of stresses transfer to the piezoresistive element, which in turn can lead to a scaling error.
2) Cracking of the piezoresistive element due to excessive fatigue or shock can lead to a scaling error and, in extreme cases, a complete failure.
3) Loss of contact between the element and the lead wires or electrodes can lead to intermittent or complete failure of the sensor.
4) Temperature variations can lead to a change in the electromechanical properties of the element, leading to bias in the readings.

E. Resistive Strain Gage

Resistive strain gages rely upon the change in the resistance due to the dimensional changes in the material (as opposed to change in material characteristics for piezoresistive materials) [9]. These gages consist of a grid of very fine wire or foil bonded to a backing (Fig. 5). The electrical resistance of the grid varies linearly with strain. Strain gages are good for detecting local strains, but have lower gage factors than the piezoresistive gages, which is compensated for by making them larger in size. They can generally be used only in applications which are static or have low vibration frequencies. Strain gages are also used in load cells or pressure transducers by measuring the stresses in the diaphragm, and in some cases, for measuring temperatures [5].

Faults in Strain Gages:

1) Gaps in the bonding layer between the strain gage and the substrate lead to either bias or scaling error, depending on the nature of the void. Debonding of the gage will result in the same faults. This is of critical importance since the bond area in a strain gage is much larger than that in piezoresistive or piezoelectric sensors [6].

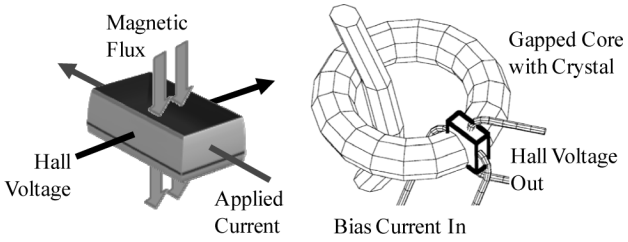

Fig. 6. (a) Hall effect in a conductor. (b) Hall effect current sensor [4].

2) Fatigue of the wire or foil can lead to cracks, causing either bias or scaling (change of gage factor) fault. In extreme cases, complete failure may occur [13].
3) Temperature variations between the loaded and the temperature-compensated strain gage can lead to bias [13].
4) Loss of contact between the lead wires and the tabs on the strain gage leads to intermittent or complete failure of the sensor.

F. Hall Effect Sensors

A voltage potential V_H, called Hall voltage, appears across a conductor when a magnetic field is applied at right angles to the current flow. Its direction is perpendicular to both the magnetic field and the current and its magnitude is proportional to both the magnetic flux density and the current (see Fig. 6).

The magnetic field causes a gradient of carrier concentration across the conductor. A larger number of carriers on one side of the conductor, compared to the other side, causes a voltage potential V_H, [4]. Typically, a ferrite crystal around a current carrying conductor is used to concentrate the magnetic field of the current, around a sensor. A bias current is then applied to the sensor and Hall voltage measured, which is proportional to the current in the main conductor. A Hall effect displacement sensor can utilizes a Hall sensor and a movable magnet, with an output proportional to the distance between the two.

Faults in Hall Effect Sensors:

1) Flaws in the core, such as degradation (corrosion, cracks), residual magnetic fields, or core breakage can result in a bias.
2) Changes in the bias current through the sensor can result in bias or scaling.
3) Temperature variations can change the magnetic properties of the ferrite core, resulting in decrease (or increase) of the induced magnetization, causing a bias in the readings.
4) Changes in the orientation of the induced magnetic field in the sensor (due to mechanical shocks or other reasons) can change the value of Hall voltage and lead to a scaling error.

G. Magnetostrictive Sensor

Ferromagnetic materials such as iron and nickel display the property of magnetostriction, where application of a magnetic field causes a strain in the crystal structure, resulting in a change in size and shape of the material [4]. To measure displacement, a moving magnet forms the "target," marking the position. The magnet's field, acting on a magnetostrictive wire, creates an ultrasonic pulse in the wire when a current pulse is passed through

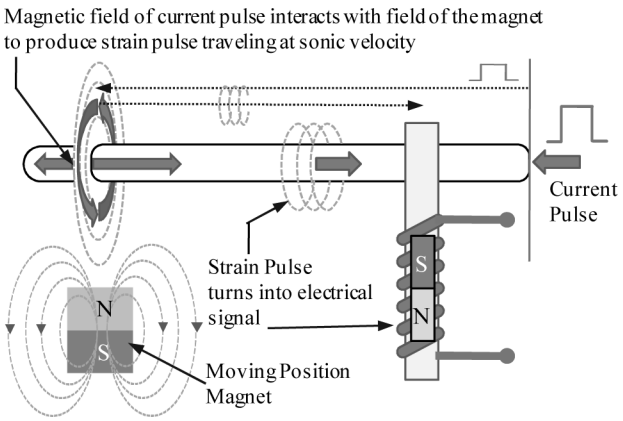

Fig. 7. Magnetostrictive principle for displacement measurement [14].

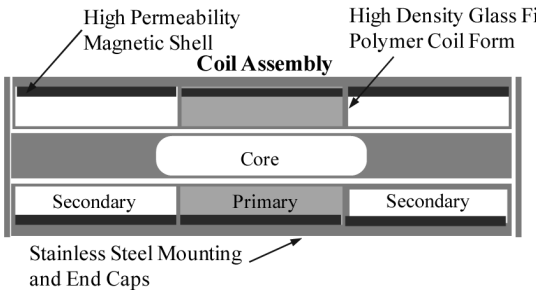

Fig. 8. Construction of an LVDT [4].

the wire. The time interval from the current pulse to the detection of the ultrasonic pulse at the end of the wire is used to determine the position of the magnet along the wire (Fig. 7) [9].

Faults in Magnetostrictive Sensors:

1) Changes in temperature cause a change in the velocity of propagation of sound through the magnetostrictive wire, which can lead to bias. Temperature also changes the magnetostrictive properties of materials, resulting in bias [15].
2) Degradation (corrosion) of the ferromagnetic wire can lead to changes in the magnetostrictive and ultrasonic properties, resulting in bias.
3) Loss of contact at the receiving end for the strain pulses can result in intermittent or complete failure.
4) Stray magnetic fields (particularly strong fields) can cause a random error in readings or result in excessive noise.

H. Linear Variable Differential Transformer (LVDT)

An LVDT is a position-to-electrical sensor whose output is proportional to the position of a movable magnetic core. The core moves linearly inside a transformer consisting of a central primary coil and two outer secondary coils wound on a cylindrical form (Fig. 8). The secondary windings are wound out of phase with each other. Moving the core results in a differential voltage between secondary coils, which varies linearly with the core's position [5]. The LVDT can be coupled with a spring-mass system to detect the displacement of the spring and measure acceleration or force [4].

Faults in LVDTs:

1) Short in one of the coils can lead to either a bias or complete failure of the sensor.

TABLE I
TYPICAL RANGES FOR SENSOR FAILURE VALUES AS AVAILABLE FROM THE LITERATURE

Fault	Range	Median	Remarks	Sensors & References
Bias	1.2% to 60%	20%	% change over the nominal value	air flow [16] temperature, fuel flow, rotor speed [17]
Scaling	0.3 to 0.7	0.45	Scale Factor	piezoelectric [10, 12] accelerometers [1]
	2.5 to 4.8	3.28	Scale Factor	accelerometers [1]
Drift	6% to 75%	29%	% change over the nominal value, reported at the end of the drift (or data set)	fuel flow [16] temperature [17]
Noise	2.5% to 250%	20%	% peak to peak values over the nominal value	pressure temperature, fuel flow, rotor speed [18] accelerometers [19] gyroscope [20]
Intermittent Dropout	2 to 10 drops	8 drops	Over a range of 20% to 29% of the reported data set, with median range of 23%	fluid flow [16]

2) Leakage of magnetic fields between the secondary coils can lead to a bias [5].
3) Changes in the primary voltage lead to a smaller induced voltage in the secondary, leading to a scaling error.

Table I summarizes the range and median values for the different fault classes found in the literature. It is hoped that this will provide an aid in modeling sensor faults with realistic magnitudes when superimposed onto real data. It will also allow simulation of diverse sets of sensor faults and subsequent training of algorithms to detect and distinguish them from system component faults. The number of references in literature showing actual sensor faults is found to be very limited; hence we list these statistics for a range of different sensors.

IV. SENSOR FAULT DETECTION AND IDENTIFICATION (FDI) TECHNIQUES

The problem of fault detection and disambiguation has been approached from various angles in the past three decades. A wide variety of techniques have been reported; they can, however, be categorized into four basic categories. The emphasis on each of these categories has changed with time and all come with their own strengths and shortcomings. A brief overview of the approaches is presented next.

Most of the early work has focused on model-based sensor fault detection and disambiguation methods which, in general, require mathematical models of the system under investigation and utilize analytical redundancy generated by these models [3], [21]. The majority of model-based approaches first compare the observed sensor output and parameter estimates obtained from the model to compute residuals. There are few distinct categories for such approaches [22]. Parity methods compute a residual vector that is zero when no fault is present and nonzero

otherwise. The various parity approaches include Parity Space Approach (PSA) [23], Parity Equation Approach (PEA) [24], Generalized Likelihood Ratio Test (GLT), and Least Square Residual Approach (LSRA). Another approach is based on Bank of Observers (state estimators) that offer to cancel out the contribution of noise and model inaccuracies [25]–[27]. State estimation approaches based on Kalman filters generate an estimate that can be used to compute residuals by comparing it with measured states [28], [29]. Other model-based approaches include fault detection filters [3] and parameter identification [30] which model various faults and track corresponding model parameters. As it is often the case, performance of analytic redundancy-based FDI techniques is limited by modeling uncertainties.

In the recent years, a notable emphasis has been placed on data-driven methods as well, where signal processing and artificial intelligence techniques are combined. Such techniques are especially important in situations where the complexity of the system makes it difficult to model. Data-driven methods are relatively simpler and quicker to implement than the model-based ones. Features are computed using standard statistical estimates or utilizing specialized domain knowledge [31], [32]. Various machine learning approaches, like artificial neural networks (ANNs), are very popular in the literature. Furthermore, approaches based on expert systems, where historical data is used to construct a set of rules to diagnose system and sensor faults, have also been used. Hybrid methods have been developed to complement various individual techniques. For instance, in [24] authors propose a hybrid method that combines Parity Equation Approach (PEA) with wavelet-based signal processing to avoid the need of a mathematical model of the aircraft. A pseudo model-based approach based on principal component analysis (PCA) has been proposed in [29], where PCA is used to compute residuals in the absence of a mathematical model.

Overall, it appears that the emphasis has been placed on generic fault detection techniques, borrowing ideas from system diagnostics. The efforts on detecting specific sensor faults are, however, less evident. In the absence of real sensor fault data, it may be desirable to create sufficiently high-fidelity fault scenarios and, using them, develop more robust solutions for sensor fault detection and disambiguation from system faults. That will, in turn, improve confidence in the overall system diagnostics.

V. Experimental Setup

A ballscrew electromechanical actuator was used as the plant in our experiments. The experiments were performed on a test stand located at Moog Inc., where the test actuator (Moog MaxForce 883-023) was connected to a hydraulic load cylinder by a rotating horn. Control and data acquisition were performed by real-time software running on dSPACE platform. Table II contains a list of all of the sensors used on the test platform, as well as their associated sampling frequencies.

Vibration was measured at four points on the test actuator, as shown in Fig. 9. All three axes of vibration were measured, with an additional measurement in the Z-direction by the accelerometer mounted directly on the nut of the ball screw. Temperature measurements were provided by a T-type thermocouple on the nut and an RTD embedded in the stator of the motor, as shown in. Fig. 9. Load is sensed by a Model 75 Sensotek 50 000 lbf. load cell. The position of the rod end of the test actuator was measured by a Trans-Tek 0219-0000 Linear Differential Voltage Transducer (LVDT).

TABLE II
List of Sensors

Measurement	Sensor	Type	Sample Rate
Load	Model 75 Sensotec Load Cell	Bonded foil strain gage compression and tension	3 kHz
Position	Trans-Tek 0219-0000	LVDT	3 kHz
Nut Temperature	T-type Thermocouple	Copper-constantan thermocouple	3 kHz
Motor Temperature	Integrated Stator RTD	RTD (thermistor)	3 kHz
Torque Producing Current	T200 Motor Drive Output	Hall effect sensor	3 kHz
Motor Velocity	T200 Motor Drive Output	Resolver	3 kHz
3-Phase Currents	(3) LEM LA 25-P Current Transducers	Closed loop (compensated), works on Hall effect	24 kHz
X-Y-Z Accelerometers	(3) PCB Model 352A24	Piezoelectric ceramic, shear	24 kHz
Nut Accelerometer	PCB Model 352A24	Piezoelectric ceramic, shear	24 kHz

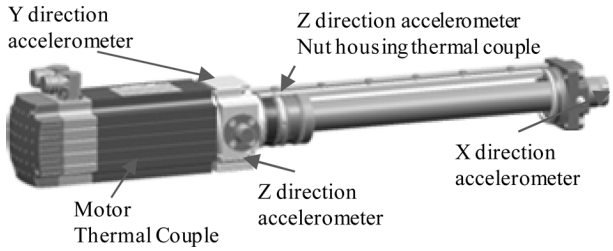

Fig. 9. Location of sensors on Moog MaxForce 883-023 actuator.

LEM LA 25-P current transducers were used on each motor phase to sense the phase currents. For data acquisition, the Moog T200 motor drive output an analog signal representing the torque producing current, as well as the motor velocity.

A. Tests Performed

Table III describes the types of mechanical component fault cases introduced during the tests.

Sensor faults were injected *a posteriori*, as described in the next section. Permutations of the following conditions were used to run $2 \times 2 \times 2 = 8$ scenarios for each of the mechanical component fault cases:

Motion profile: sinusoid or triangular wave.

Load type: constant or spring.

Load level: low (860 lbs spring force, 900 lbs constant force) or high (1725 lbs spring force, 1800 lbs constant force).

For the purposes of training and testing the neural network-based classifier (described in the subsequent sections) extended duration scenarios were created using the collected data. These scenarios were designed to preserve the character of the collected data as much as possible, while extending the duration

TABLE III
SEEDED MECHANICAL COMPONENT FAULT EXPERIMENTS

Experiment Set	Description
Baseline	Data collected with a nominal actuator just before the first set of ball return jam tests.
One Ball Return Jammed	One of the return channels fully blocked. Simulates obstruction of the return channel by a detached piece of insulation or other debris.
Repeatability	Tests to determine whether disassembly and reassembly of actuators affects test results. Five back to back runs were conducted.
Backlash	Tests with undersized balls to simulate backlash (freeplay)
Spalling	The purpose of this series of tests was to determine if a surface flaw (spall) can be detected using the actuator sensor suit. Three flaws have been electro-discharge machined into the screw of the actuator. The flaws were machined into the entire root of the screw forming a continuous flaw from crest to crest.

to 180 seconds. They contain two segments each—nominal, to represent a healthy system before the fault occurred, and faulty (90 seconds per segment). Since the hardware limitations of the test stand required that the faults be seeded before the corresponding experiments began, nominal data was chosen from experiments conducted under the same conditions. The total number of scenarios produced was 48: (8 conditions) × (2 components faults + 4 sensor faults).

VI. SENSOR FAULT SIMULATIONS

Bias: in our experiments bias, injected into the nut temperature sensor data, was specified as percentage of the average baseline temperature (80 F), calculated over the set of nominal (no fault injected) scenarios. Gaussian noise was then introduced into the actual amount of bias added, with a signal-to-noise ratio (SNR) of 5 (see Fig. 10).

Drift: this fault was also injected into the nut temperature data. The fault was defined by specifying drift velocity (distance traveled in a certain period of time). The length of constant drift velocity segments was randomized (maximum 1000 data points) and Gaussian noise introduced into velocity value itself—so for each segment the velocity may be somewhat different from its neighbors. The SNR for the later was set to 5.

Scaling: the signal is amplified by a scaling factor, also with Gaussian noise injected (SNR of 5).

Loss of Signal: sensor data from the point of failure replaced by all zeros.

VII. CLASSIFIER DIAGNOSTICS SYSTEM

Taking into account the complexity of the experimental data and the assortement of failure modes, a diagnostic system based on ANNs was designed. A comprehensive analysis of the data was carried out to extract a set of uncorrelated features that would not only detect the various fault modes but also disambiguate between sensor and system faults. Keeping this requirement in mind, a confusion matrix was created and partitioned into sections that helped to interpret results accordingly (Table VI, described further in part C). The present section explains the implementation details and enumerates the key aspects of the classifier diagnostic system.

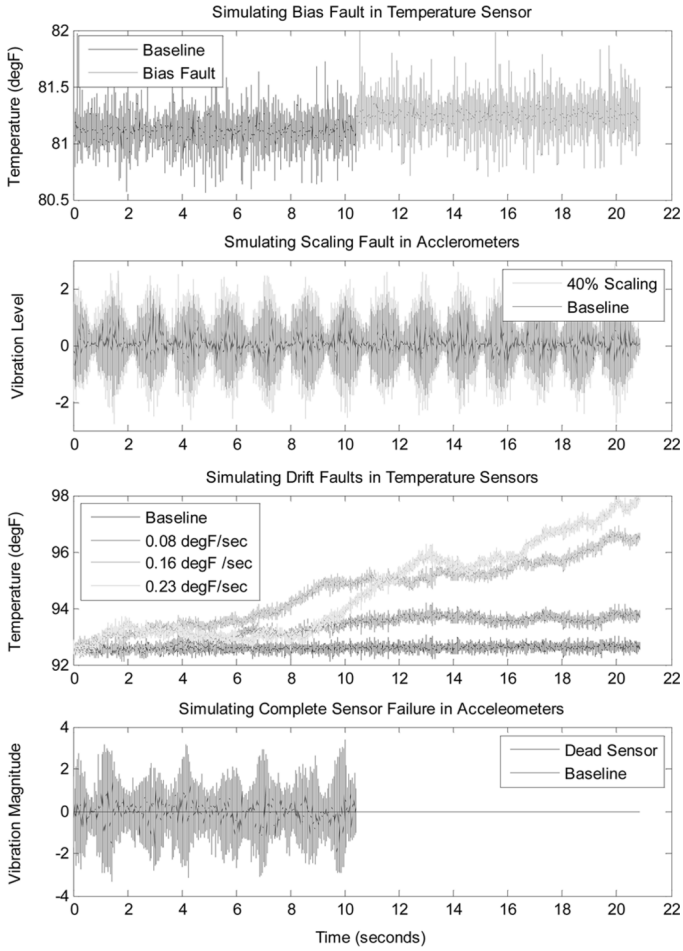

Fig. 10. Sensor fault simulations.

TABLE IV
FAULT VERSUS FEATURE MATRIX

Faults	Features					
	TD_{Nut}	TD_{Motor}	SD_x	SD_y	SD_Z	DI
Return Channel Ball Jam	X	X	X	X	X	
Spall			X	X	X	
Nut thermocouple Drift	X					X
Nut thermocouple Bias	X					
Z Accel. Scaling					X	
X Accel Complete Failure			X			

A. Feature Extraction

Feature extraction is one of the most important steps in building a successful (accurate and reliable) diagnostic system. To achieve a successful practical implementation, it is desirable that features not only be computationally inexpensive, but also explainable in physical terms. Furthermore, they should: a) be characterized by large between-class and small within-class

TABLE V
CLASSIFIER INPUT FEATURES TYPES

Feature Type	Sensors	Definition	Fault Modes	Rationale
Temperature Deviation (TD)	Nut thermocouple, Motor thermocouple	Absolute deviation from the nominal temperature range	Spall, jam, sensor bias	Nut temperature rises due to increased friction from spalled nut. Motor temperature rises due to increased current levels to counter increased resistance. Temperatures also change due to bias.
Drift Indicator (DI)	Nut thermocouple, Motor thermocouple	A binary feature that assumes the value of *one*, if a finite rate of change of temperature is detected within the sampling window, and *zero* otherwise	Sensor drift	Monitoring over some period of time can help identify sensor drift and distinguish it from bias, which is not expected to change continuously in shorter time intervals.
Signal Standard Deviation (SD)	Accelerometers: X, Y, Z on motor housing and one on the Nut	Standard deviation of the signal within one sampling window	Jam, dead sensor	A jam manifests itself in increased vibrations measured by the accelerometers. A dead sensor results in zero magnitude output.
Load Profile Indicator	Position sensor	Characterizes the smoothness of load profiles ranging between smooth sinusoids to rough triangular profiles	All	Nature of the load profile significantly changes the vibration signature of the system. This difference should be distinguished from failure signatures.
Force Indicator	Position sensor	Assesses the force on actuator. For opposing force motion the force remains constant, proportional to peak loads. For spring motion force varies with the position and is a fraction of the peak loads	All	Given the combinations of two different load conditions and two load application methods, differences in corresponding sensor signatures should be distinguished from fault signatures.

variance; b) be fairly insensitive to external variables like noise; and c) uncorrelated with other features. Keeping these criteria in mind, we selected a set of seven features (Temperature Deviation and Drift Indicator on the ballscrew nut and motor housing thermocouples; Standard Deviation on the X, Y, and Z accelerometers) that were expected to detect and distinguish between a healthy system, two actuator fault modes, and four sensor faults (see Table IV).

In addition, two extra features were designed to characterize those experimental conditions that considerably affect sensor measurements—load profile and axial force magnitude. Features were calculated every half a second within a 1 s long sliding window. Thus, for each 90 seconds long segment 180 feature points were obtained. The features are described in Table V.

B. Diagnostic Classifier

A multicategory classifier was implemented using a three layer ANN. The first layer consisted of nine nodes, with *tansigmoid* transfer functions, one for each feature in the input feature vector. The hidden layer had five nodes with *logsigmoid* transfer functions and the output layer had seven nodes with *logsigmoid* transfer functions—one for each of the seven classification categories. All input features were continuous, real-valued, and were standardized to have zero-mean and unit variance [33]. Binary targets were assigned such that of the seven output bits only the correct category bit would be set 1 and the rest would remain 0. Initial weights for the network were chosen based on standardized input ranges in order to ensure uniform learning [33]. Networks were trained using the resilient backpropagation (RPROP) algorithm [34].

TABLE VI
CONFUSION MATRIX FOR TWO COMPONENT FAULTS (CF) AND FOUR SENSOR FAULTS (SF)

		NF	CF1	CF2	SF1	SF2	SF3	SF4
NI	NF	TP	FP					
	CF1	FN	TP		MC			
	CF2			TP				
	SF1		MC		TP			
	SF2					TP		
	SF3						TP	
	SF4							TP

C. Evaluation Procedure

Data was divided into two sets for training and testing purposes, based on the load levels. The classifier was trained on low load conditions ($\sim$900 lbs) and tested with high load ($\sim$1800 lbs) conditions. In order to obtain a meaningful statistic, 30 ANNs were trained and tested for each experiment and the results averaged. Training was carried out for 200 epochs. Results were further aggregated in the form of a confusion matrix (as shown in Table VI) in order to observe the true positive (TP), false positive (FP), false negative (FN), misclassification (MC), and nonidentification (NI) rates. NF stands for no-fault.

As expected, it was observed that detection and disambiguation performance varied with changing sensor fault magnitudes. Therefore, sensitivity analysis was carried out to characterize the effect of varying them. Fault parameters for drift, bias, and scaling were adjusted one at a time over a wide range of values, while keeping the other fault parameters fixed at predetermined levels (derived from typical ranges available from the literature). More specifically, these predetermined values are temperature bias fixed at an offset of 100% of peak-to-peak magnitude, temperature drift fixed at 0.02 ° F/s, and scaling fixed

TABLE VII
RANGES OF SENSOR FAULT PARAMETER VARIATION FOR CLASSIFIER SENSITIVITY ANALYSIS

Sensor Fault	Min Value	Max Value
Bias	0	500% of peak-to-peak magnitude offset
Drift	0.005 °F/sec	0.25 °F/sec
Scaling	0.1x	5x

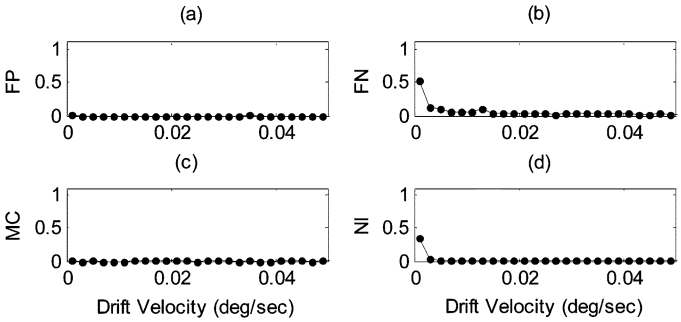

Fig. 11. Sensitivity of the classifier as drift velocity parameter changes.

at 1.5 times. The ranges of variation for these parameters are shown in Table VII.

VIII. RESULTS AND DISCUSSION

Results were aggregated in two ways. First, performance was evaluated in terms of sensitivity of metrics (FP, FN, MC, and NI) from the classifier for individual sensor faults. Therefore, if parameters for a sensor fault f_i, were varied, the effect was recorded only on the performance of classifier in classifying f_i, even though all other (system and sensor) fault modes were also present. Second, an overall performance assessment was made and an aggregate number was recorded for total FP, FN, MC, and NI rates for all faults combined, as the intensity of a single sensor fault f_i was varied. The metrics for individual sensor faults are defined as follows.

False Positive: Sensor fault f_i is reported when no fault present.
False Negative: No fault reported when a sensor fault f_i present.
Misclassification: A system fault reported when sensor fault f_i present or sensor fault f_i reported when a system fault is present.
Nonidentification: A fault detected but not identified when sensor fault f_i is present.

As shown in Fig. 11, the diagnostic classifier implemented in this study is slightly sensitive to small drifts. For small drifts it becomes difficult to disambiguate between drift fault and nominal behavior, resulting in a higher false negative rate. The overall detection and disambiguation performance is within 5% FP, within 4% FN, less than 2% MC, and NI generally less than 8% except for low drift velocities where it is as high as 16%, in some cases.

Fig. 12 shows the classifier performance for bias sensor fault. Here, the sensitivity of the classifier can clearly be seen and attributed to two factors. First, as mentioned above, for there is a high false negative rate for low bias cases, as it is difficult to distinguish from baseline data. Second, several fault modes (i.e., ball jam and spall) also result in increased operating temperatures, just like bias. However, since jam and spall are also

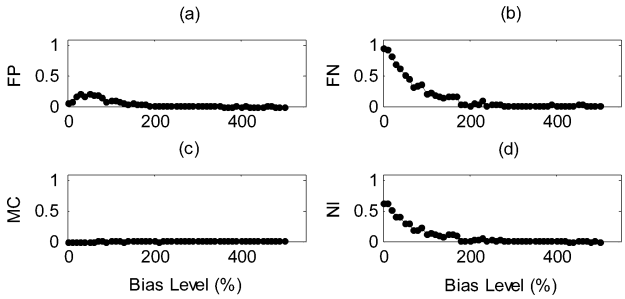

Fig. 12. Sensitivity of the classifier bias parameter changes.

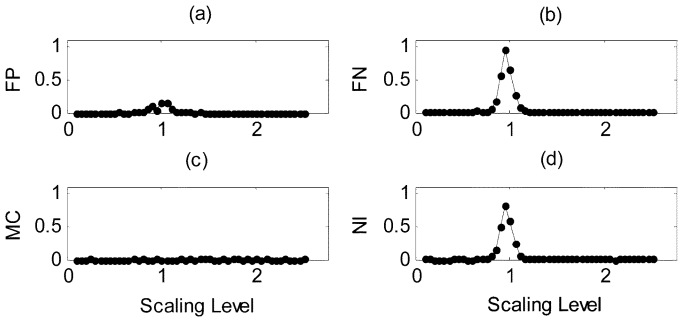

Fig. 13. Sensitivity of the classifier as scaling parameter changes.

reflected in other features that do not trigger in the presence of bias, a high nonidentification rate is also observed. In terms of overall performance, once again, less than 4% FP and FN are observed whereas NI goes as high as 18% for low values of bias. Misclassification rate is negligible.

As expected, scaling fault detection performance deteriorates as the scaling coefficient gets close to one (Fig. 13). For the scaling case, the overall NI rate was observed as high as 29% with scaling coefficients close to one. FP rates remained low (within 5%), FN within 4%, and MC less than 1%, when combined for all fault scenarios.

Therefore, it can be concluded that in this study, the overall performance of the classifier remains consistent with low FP, FN, and MC rates varying in the range of 0%–7%, except for the NI rate, which becomes high in the more sensitive ranges for all three sensor fault modes. Features are needed that are less sensitive to fault intensity parameters. The sensitivity analysis performed provides a useful insight into the fault classification problem, where a classifier must be evaluated for all possible fault scenarios and designed to provide a more robust diagnosis.

IX. PLANS FOR FUTURE WORK

There is a number of possible avenues for future work on this topic. First, the set of sensors needs to be widened from the current set taken from a fairly narrow application domain. Additional fault modes need to be considered as well. While we have constrained this investigation to faults occurring within the sensors themselves, a large number of sensor-related faults are due to data acquisition circuitry (analog-to-digital converters, signal conditioning), electrical systems supporting sensor operation (power supplies), and other sources. Moreover, some sensor fault types, such as intermittencies, should be the subject of a closer examination, since they are responsible for

a large number of problems in fielded systems. A number of physics model-based and probabilistic approaches is currently being considered for handling intermittent faults. One them is a model-based, finite-state diagnostic system which will either supplement or incorporate the current neural network reasoner. Such a model-based system would be based on a state machine where each state node describes a particular nominal or fault mode via a set of equations and constraints. Transitions between the modes can be conditionalized as well. Once the neural network component detects a fault condition and the state machine is transitioned into the appropriate mode, the subsequent indications are checked to decide whether the mode should be exited in favor of a different one. The time spent in various fault modes (as well as the time spent in between reentering the same fault mode) can be reported to determine the degree of fault intermittency.

While in this work we studied a classifier system that distinguished between sensor faults and system faults, it should be investigated how such classifiers (or reasoners) can be scaled to deal with large systems. This can be accomplished by a system-of-systems approach, by developing sensor fault tolerant schemes, or by modeling explicit or implicit function or analytical redundancies. While the features described herein focused mostly on the time domain, other features (e.g. frequency-domain) should be considered. In practice, sensor fault detection should go hand-in-hand with accommodation strategies. The understanding gained in the underlying mechanisms of sensor faults should be tapped into when considering new techniques for sensor fault accommodation and will hopefully aid in making system health management a more viable technology overall.

Another avenue for future work is verification of sensor fault models developed. Experiments with seeded faults should be conducted on realistic systems to confirm that the models behave correctly. To that end, plans are under way to carry out sensor fault experiments on the new actuator test stand at NASA Ames by inducing certain types of faults in the sensors and observing their signatures while the system operates under a variety of load conditions. Among other objectives, the stand will aid in diagnostic and prognostic work for position measurement devices, such as LVDTs and resolvers/encoders, as one of its key features is an external, high-precision laser-triangulation position sensor.

X. Conclusion

This paper examined the physical underpinnings of sensor faults and mapped them to five general categories. The ultimate goal was to enable better systems health management by providing an insight into behavior of faulty sensors (as opposed to treating them as black boxes) which, in turn, might lead to improved fault accommodation strategies. In that spirit, a fault detector/classifier has been demonstrated that successfully handles the set of faults for a wide range of fault parameters. A large part of the work was devoted to sensitivity analysis of the classifier to variations of these parameters and identification of regions where suboptimal classification results could occur. The approach utilized for the analysis may suggest a general methodology for developing and testing diagnostic systems suitable for a wider range of sensor faults. A comprehensive analysis of the physical causes of sensor faults will also contribute to improved robustness of system health management reasoners.

Acknowledgment

The authors would like to extend their gratitude to colleagues at the Prognostic Center of Excellence (NASA Ames Research Center) for their extensive assistance with this research and preparation of the manuscript. They would also like to thank P. Stoelting and J. Rack at Moog Corporation for their efforts in producing and analyzing experimental data used in this project.

References

[1] D. C. Zimmerman and T. L. Lyde, "Sensor failure detection and isolation in flexible structires using the eigensystem realization algorithm," in *Proc. 33rd Structural Dynamics and Mater. Conf.*, Dallas, TX, 1992, pp. 2156–2166.

[2] S. S. Iyengar and L. Prasad, "A general computational framework for distributed sensing and fault-tolerant sensor integration," *IEEE Trans. Syst., Man, Cybern.*, vol. 25, no. 4, pp. 643–650, 1995.

[3] J. J. Gertler, "Survey of model-based failure detection and isolation in complex plants," *IEEE Control Syst. Mag.*, p. 11, Dec. 1988.

[4] J. G. Webster, *The Measurement, Instrumentation, and Sensors Handbook*. Boca Raton, FL: CRC Press, 1999.

[5] J. S. Wilson, *Sensor Technology Handbook*. Burlington, MA: Elsevier, 2005.

[6] Omega Technical Reference, 2008-09-22. [Online]. Available: http://www.omega.com/techref/

[7] J. G. Ternan, "Thermoelectric drift of thermocouples due to inhomogeneous changes in composition," *J. Appl. Phys.*, vol. 55, no. 1, pp. 199–209, 1983.

[8] T. Hamada and Y. Suyama, "EMF drift and inhomogeneity of type K thermocouples," in *Proc. SICE 2004 Annu. Conf.*, Sapporo, Japan, 2004, pp. 989–992.

[9] R. H. Bishop, *The Mechatronics Handbook*. Boca Raton, FL: CRC Press, 2002.

[10] L. Tong, D. Sun, and S. N. Atluri, "Sensing and actuating behaviours of piezoelectric layers with debonding in smart beams," *Smart Mater. Structures*, vol. 10, pp. 713–723, 2001.

[11] C. Li and G. J. Weng, "Antiplane crack problem in functionally graded piezoelectric materials," *J. Appl. Mech.*, vol. 69, pp. 481–488, 2002.

[12] D. Wang, Y. Fotinich, and G. P. Carman, "Influence of temperature on the electromechanical and fatigue behavior of piezoelectric ceramics," *J. Appl. Phys.*, vol. 83, no. 10, pp. 5342–5350, 1998.

[13] Strain Gage Knowledge Base—Technical Notes, 2008-09-23. [Online]. Available: http://www.vishay.com/strain-gages/knowledge-base-list/

[14] MTS Systems Corporation [Online]. Available: http://www.mtssensors.com/ 2008-09-24

[15] A. E. Clark *et al.*, "Magnetostrictive properties of body-centered cubic Fe-Ga and Fe-Ga-Al alloys," *IEEE Trans. Magn.*, vol. 36, no. 5, pp. 3238–3240, 2000.

[16] K. Goebel and W. Yan, "Correcting sensor drift and intermittency faults with data fusion and automated learning," *IEEE Syst.*, vol. 2, no. 2, pp. 189–197, 2008.

[17] S. J. Qin and W. Li, "Detection and identification of faulty sensors with maximized sensitivity," in *Proc. 1999 Amer. Control Conf.*, vol. 1, pp. 613–617.

[18] P.-J. Lu and T.-C. Hsu, "Application of autoassociative neural network on gas path sensor data validation," *J. Propulsion and Power*, vol. 18, no. 4, pp. 879–888, 2002.

[19] D. C. Zimmerman and T. L. Lyde, "Sensor failure detection and isolation in flexible structures using system realization redundancy," *AIAA J. Guidance, Control and Dynamics*, vol. 16, no. 3, pp. 490–497, 1993.

[20] C. D. Neppach and V. A. Casdorph, "Sensor failure detection, identification and accommodation in a system without sensor redundancy," *AIAA J. Control Dynamics*, vol. 18, no. 6, pp. 1280–1286, Nov.-Dec. 1995.

[21] G. Rizzoni and P. S. Min, "Detection of sensor failures in automotive engines," *IEEE Trans. Veh. Technol.*, vol. 40, no. 2, pp. 487–500, 1991.
[22] S. Simani, C. Fantuzzi, and S. Beghelli, "Diagnosis techniques for sensor faults of inustrial processes," *IEEE Trans.n Control Syst. Technol.*, vol. 8, no. 5, pp. 848–855, 2000.
[23] J. J. Gertler, "Fault detection and isolation using parity equations," *Control Engineering Practice*, vol. 5, no. 5, pp. 653–661, 1997.
[24] S. Kim *et al.*, "Hybrid fault detection and isolation techniques for aircraft inertial measurement sensors," *KSAS Int. J.*, vol. 7, no. 1, pp. 73–83, 2006.
[25] W. Chen and M. Saif, "A sliding mode observer-based strategy for fault detection, isolation, and estimation in a class of Lipschitz nonlinear systems," *Int. J. Syst. Sci.*, vol. 38, no. 12, pp. 943–955, 2007.
[26] C. P. Tan and C. Edwards, "Sliding mode observers for detection and reconstruction of sensor faults," *Automatica*, vol. 38, pp. 1815–1821, 2002.
[27] E. Kiyak, Ö. Çetin, and A. Kahvecioglu, "Aircraft sensor fault detection based on unknown input observers," *Aircraft Eng. Aerosp. Technol.*, vol. 80, no. 5, pp. 545–548, 2008.
[28] F. Gustafsson, "Stochastic fault diagnosability in parity spaces," in *Proc. 15th IFAC World Congr.*, Barcelona, Spain, 2002.
[29] A. Hagenblad, F. Gustafsson, and I. Klein, "A comparison of two methods for stochastic fault detection and principal component analysis," in *Proc, 13th IFAC Symp. Syst. Id. (SYSID)*, Rotterdam, The Netherlands, 2003, pp. 27–29.
[30] J. Litt, M. Kurtkaya, and A. Duyar, "Sensor fault detection and diagnosis simulation of a helicopter engine in an intelligent control framework," *NASA TM* 106 784, Nov. 1994.
[31] P. Seda, E. Kadir, and B. Emine Dogru, "Intelligent sensor fault detection and identification for temperature control," in *Proc. 11th WSEAS Int. Conf. Comput.*, Agios Nikolaos, Greece, 2007, pp. 131–134.
[32] S.-J. Kim and C.-W. Lee, "Diagnosis of sensor faults in active magnetic bearing system equipped with built-in force transducers," *IEEE Trans. Mech.*, vol. 4, no. 3, pp. 180–186, 1999.
[33] R. O. Duda, P. E. Hart, and D. G. Stork, *Pattern Classification*, 2nd ed. New York: Wiley, 2000, pp. 654–.
[34] M. Riedmiller and H. Braun, "A direct adaptive method for faster backpropagation learning: The RPROP algorithm," in *Proc. IEEE Int. Conf. Neural Networks*, San Fransisco, CA, 1993, pp. 586–591.

Edward Balaban (M'08) received the B.S. degree in computer science from The George Washington University, Washington, DC, in 1996 and the MS. degree in electrical engineering from Cornell University, Ithaca, NY, in 1997.

He is a Researcher in the Diagnosis and System Health Group at NASA Ames Research Center. His main areas of interest are diagnostics and prognostics of physical systems. He is currently the lead for actuator prognostics with the Diagnostics and Prognostics Group in the Intelligent Systems Division. During his years at Ames Research Center, he participated in research and development of diagnostic and other autonomy elements for the X-34 experimental reusable launch vehicle, International Space Station, robotic astronaut assistants, autonomous planetary drills, and the future generation of autonomous micro-spacecraft.

Abhinav Saxena (M'06) received the B.Tech. degree in 2001 from the Indian Institute of Technology (IIT) Delhi, the M.S. degree in 2003 and the Ph.D. degree in electrical and computer engineering from the Georgia Institute of Technology, Atlanta.

He is a Staff Scientist with the Research Institute for Advanced Computer Science, Prognostics Center of Excellence, NASA Ames Research Center. His research focus lies in developing prognostic algorithms for engineering systems.

Prasun Bansal received the M.S. degree in aeronautics and astronautics from Stanford University, Stanford, CA, in 2008 and the B.Tech. degree in mechanical engineering from the Indian Institute of Technology (IIT), Delhi, in 2006.

He is an intern with Mission Critical Technologies at the Prognostics Center of Excellence, NASA Ames Research Center. His research focus lies in design and development of engineering systems and multidisciplinary optimization.

Kai Goebel (M'08) received the Diplom-Ingenieur degree from the Technische Universität München, Germany in 1990, and the M.S. and Ph.D. degrees from the University of California at Berkeley in 1993 and 1996, respectively.

He is a Senior Scientist at NASA Ames Research Center, where he leads the Diagnostics and Prognostics Groups in the Intelligent Systems Division. In addition, he directs the Prognostics Center of Excellence and he is the Associate Principal Investigator for Prognostics for NASA's Integrated Vehicle Health Management Program. He worked at General Electric's Corporate Research Center, Niskayuna, NY, from 1997 to 2006, as a Senior Research Scientist. He has carried out applied research in the areas of artificial intelligence, soft computing, and information fusion. He holds ten patents and has published more than 100 papers in the area of systems health management. His research interest lies in advancing these techniques for real-time monitoring, diagnostics, and prognostics.

Simon Curran received the B.S.E.C.E. degree in 2005 and the M.S.E.C.E. degree in 2007 from Ohio State University, Columbus.

His research focused on intelligent control and humanoid locomotion. While at Ohio State University, he served as an Assistant Lecturer for The Fundamentals of Engineering for Honors Program (FEH). Presently, he works with the Aircraft System's Group, Moog Inc. His current interests are neural network applications for machine anomaly detection and network fusion.